Bow-Echo Mesovortices: A Review

Alexander D. Schenkman[1*] and Ming Xue[1,2]
Center for Analysis and Prediction of Storms[1] and School of Meteorology[2]
University of Oklahoma, Norman Oklahoma 73072

Submitted July 2015, Revised: September 2015
Atmospheric Research

1

Abstract

Non-supercellular damaging winds from convective storms are overwhelmingly associated with quasi-linear convective systems. A review of early studies of these systems suggested that wind damage/speed was not continuous and instead was enhanced over many small areas. More recent research has revealed a close association between damaging winds, tornadoes, and low-level meso-γ-scale vortices (mesovortices) that develop within the convective portion of QLCSs. Observational and numerical studies are reviewed to explain the relationship between mesovortices, damaging winds, and tornadoes. Substantial disagreement exists with regard to the processes responsible for the genesis of these mesovortices. Nonetheless, case study simulations of real events have been successful in simulating mesovortices in both a deterministic and probabilistic framework. Implications and recommendations for future work in a warn-on-forecast context are provided.

1. Introduction

In the United States, the vast majority of non-supercellular tornadoes and damaging winds occur in meso-β-scale (20-200 km; Orlanski 1975) quasi-linear convective systems (QLCS), such as squall lines and bow-echoes (Trapp et al. 2005). The structure of bow echoes (a type of QLCS that develops into a bow-shaped radar reflectivity echo structure) and their association with damaging winds was first studied in detail by Fujita and collaborators in the late 1970s and early 1980s. Specifically, Fujita (1978) studied radar imagery and developed a conceptual model that describes the life cycle of the bow echo (Fig. 1). In this conceptual model, the system begins as a single 'tall echo' and then proceeds to develop into a 'bow echo' that eventually develops a rotating comma-echo during its mature and decay phase. Fujita (1978; 1979) identified the apex of the bow-echo as an area where a downburst, defined as a strong downdraft that induces an outburst of damaging winds on or near the ground, could lead to wind damage and possibly tornadoes.

Initial work studying the structure of bow-echoes focused on larger system-scale features such as the development of mid-level counter-rotating, or 'book-end', vortices (e.g., Weisman 1992, 1993), trailing mid-level mesoscale convective vortices (e.g., Houze et al. 1989; Johnston 1981; Jorgensen and Smull 1993; Menard and Fritsch 1989; Skamarock et al. 1994) and the rear-inflow jet (RIJ), an area of mid-level rear-to-front flow that extends from the stratiform to the convectively active portion of QLCSs (e.g., Fujita 1981; Klimowski 1994; Smull and Houze 1987). RIJs have been implicated in the production of damaging winds as well as in creating a horizontal vorticity balance that allows for long-lived bow echoes (Weisman

* Alexander D. Schenkman, Center for Analysis and Prediction of Storms, University of Oklahoma, 120 David L. Boren Blvd, Norman OK 73072, email: alex3238@ou.edu

1993).

In addition to examining the effects of the RIJ on system longevity, Weisman (1993) used idealized simulations of bow-echoes to explore the generation of bookend vortices and proposed that book-end vortices were the result of system-scale tilting of environmental vorticity by the system scale updraft and downdraft. Furthermore, Weisman (1993) pointed out that the book-end vortices acted to accelerate and focus the system's RIJ which led to severe winds at the bow-apex (Fig. 2). Weisman (1993) also suggested that more careful analysis was necessary to determine the role of the system-generated (baroclinic) vorticity. Drawing on this suggestion, Weisman and Davis (1998) set out to determine the relative contribution of the ambient and system-generated baroclinic vorticity in the development of system and sub-system scale mid-level line-end vortices (a more general term than 'bookend' for vortices that develop at the ends of convective line segments) based idealized numerical simulations and detailed diagnostic analyses. Their study determined that tilting of the system-generated vorticity was the leading order cause of system scale line-end vortices (Fig. 3). They clarified that the role of environmental shear was to promote more intense and upright upward motion along the systems leading edge thus promoting more intense vortices. Moreover, Weisman and Davis (1998) found that the cyclonic (anti-cyclonic) vortex was enhanced (weakened) by the convergence of Coriolis rotation.

Over the past two decades, higher-resolution observations, numerical simulations, and the implementation of the Weather Surveillance Radar – 1988 Doppler (WSR-88D) radar network have provided opportunities for more detailed study of the severe winds and tornadoes within larger-scale bow echoes. These studies have revealed the existence of low-level meso-γ-scale (2-20 km; Orlanski 1975) vortices (hereafter; mesovortices). These mesovortices have been found to be closely linked with swaths of high winds and tornadoes in QLCSs. It is important to distinguish that mesovortices are distinctly a low-level feature that are generally smaller in scale than book-end vortices, and may occur anywhere within the convectively-active portion of a QLCS, rather than only at the end of the line segment. Moreover, they are considerably smaller than trailing mid-level mesoscale-convective vortices (MCVs; e.g., Johnston 1981; Menard and Fritsch 1989).

The remainder of this paper will focus on reviewing the characteristics, dynamics, and successful prediction of mesovortices. In particular, section 2 will present a general overview of the observations and simulations of mesovortices and their relationship to damaging winds and tornadoes. Mesovortex genesis mechanisms will be discussed in section 3. Section 4 will examine two case studies in which mesovortices and their parent storm system were successfully predicted using high-resolution numerical simulations and data assimilation. A summary and a discussion of key results with implications for future study are presented in section 5.

2. Mesovortices, damaging winds, and tornadoes

As mentioned in the introduction, over the past 20 years, studies have noted the presence of low-level mesovortices embedded within the leading edge convection of QLCSs. The term "mesovortex" was first used in Przybylinski (1995) in reference to a strong vortex near the northern end of a rapidly moving squall line. Weisman and Trapp (2003; hereafter WT03) more formally defined mesovortices as significant *low-level* meso-γ scale vortices that form within QLCSs. They note that these mesovortices were similar in size and structure to low-level mesocyclones in supercells but differ in that they are generally not accompanied by a mid-level mesocyclone. In this section, the relationship between mesovortices, damaging winds, and tornadoes is explored by reviewing observational and modeling studies. Because the term 'mesovortex' was not formally defined until WT03, several of the cited studies used different terminology to discuss what may have been mesovortices.

2.1 Observational studies

Fujita and Wakimoto (1981) studied a damaging wind event that occurred from Chicago to Detroit on 16 July 1980. From careful analysis of damage patterns produced by the event, they identified five scales of downburst wind damage (Fig. 4). Their study noted that downbursts typically occurred in clusters with microbursts and embedded very small-scale 'burst swaths'. Fujita and Wakimoto (1981) also made a distinction between the winds associated with the gust front and the stronger winds associated with 'downbursts'. Building upon the work of Fujita and Wakimoto (1981), Forbes and Wakimoto (1983) present a detailed study of a mesoscale convective system (MCS) that produced numerous tornadoes, downbursts, and microbursts on 6 August 1977 near Springfield, IL. They found that the tornadoes and downbursts occurred in association with a bow-echo during this event. Moreover, the tornadoes seemed to be associated with downbursts as well as with the rotating comma head of the convective system. They noted that hook echoes were not observed and that the "tornadoes appeared to develop in conjunction with wind shears associated with the gust front and with microbursts." Though Fujita and Wakimoto (1981) and Forbes and Wakimoto (1983) did not have Doppler radar data to analyze the radial velocity in the storms they analyzed, the location and description of these tornadoes and downbursts suggests that the some of features they are describing were potentially related to mesovortices.

Though Fujita and collaborators cleverly deduced the wind structure in hindsight from damage surveys, a more detailed understanding of the structure of the MCS wind field required the availability of Doppler radar observations. To prepare forecasters for interpreting the operational WSR-88D Doppler radar data, Przybylinski (1995) presented a survey of bow-echoes as observed by Doppler radar systems. He noted that mesoscale vortices had been observed near the bow apex and northern end of squall lines (Burgess and Smull 1990). The greatest wind damage was generally associated with these vortices and tornadoes near the bow echo apex. Przybylinski suggested that shearing instability may be the root cause for these vortices. Trapp et al. (1999) also speculated shearing instability was responsible for the development of a series of mesovortices along the line-echo wave pattern they studied.

Radar data sets of bow echoes and mesovortices became more plentiful following the operational deployment of the WSR-88D network. Pfost and Gerard (1997) and Wolf (1998) documented two cases where tornadoes developed in association with the comma-echo phase of a QLCS. Funk et al. (1999) presented a detailed study of a derecho that occurred over Kentucky and southern Indiana on 15 April 1994. Funk et al. (1999) noted that damaging wind occurrences in this system were closely tied to the development of mesocyclone-scale vortices at low-levels at the bow-apex and associated with the comma head of the QLCS. Vortices that were longer-lived and deeper were observed to produce tornadoes and more widespread damaging wind swaths. Weaker vortices also produced damaging winds but were non-tornadic. Funk et al. (1999) also speculated that shearing instability was important in the formation these vortices.

Atkins et al. (2004; 2005) built upon the work of Funk et al. (1999) and studied the characteristics of mesovortices and their relationship to tornadoes and high winds. Specifically, Atkins et al. (2004) studied a severe bow echo that occurred in June 1998 and found that tornadic mesovortices tended to have a significantly longer life-span than non-tornadic mesovortices. Moreover, tornadic mesovortices had much stronger rotational velocities than their non-tornadic counterparts. The differences in rotational velocities were most pronounced at low levels. Based on these observations, Atkins et al. (2004) suggested it may be possible to distinguish between tornadic and non-tornadic mesovortices in an operational setting. Atkins et al. (2005), based on the study of a different severe bow-echo case, also found that tornadic mesovortices were longer-lived and stronger than non-tornadic mesovortices. Mesovortices were also observed to be coincident with most of the damaging straight-line winds produced by the bow echo studied in Atkins et al. (2005). In addition, Atkins et al. (2005) observed that tornadic mesovortices were

stronger than non-tornadic mesovortices, even prior to tornadogenesis, which could be promising for operational forecasters trying to provide accurate tornado warnings. However, Atkins et al. (2005) also found that tornadogenesis occurred, on average, only 12 min after mesovortex genesis suggesting that forecasters would have very little lead time. Finally, Atkins et al. (2005) suggested that mesovortices were more likely to become tornadic if they were in close proximity to the RIJ possibly owing to stronger stretching associated with enhanced convergence.

The link between mesovortices and damaging winds was solidified by Wheatley et al. (2006). They surveyed the MCS cases observed during the Bow Echo and Mesoscale Convective Vortex Experiment (BAMEX; Davis et al. 2004) and found that, while damaging winds occurred in MCSs that did not produce low-level mesovortices, the most intense wind damage was associated the MCSs that did produce mesovortices. Moreover, Wheatley et al. (2006) found that these intense damaging winds were generally spawned on the south side of the mesovortices. Similar results were found in the QLCS studied by Wakimoto et al. (2006a; 2006b). Additionally, Wakimoto et al. (2006b) used a flow decomposition to determine that damaging winds in mesovortices were the result of the superposition of the mesovortex flow with the rear-inflow jet (Fig. 5).

2.2 Modelling studies

Accurate numerical simulations afford the opportunity to examine dynamic relationships and parameter spaces in much more detail than observational studies. The association between mesovortices and high winds has been examined in the model simulations of WT03, Trapp and Weisman (2003; hereafter TW03), Atkins and St. Laurent (2009a), and Xu et al. (2015b). WT03 used the Klemp and Wilhelmson (1978) 3D cloud model to simulate the behavior of mesovortices in various windshear regimes. Their experiments included the impact of the intensity and depth of environmental vertical shear on mesovortex behavior. In general, WT03 found that stronger vertical shear led to stronger simulated mesovortices. This was especially the case when the shear was confined to the lowest few kilometers rather than a deeper layer (i.e., 0-7.5 km shear). They attributed this result to the fact that stronger environmental shear promoted stronger, more upright updrafts which led to more intense vortex stretching. WT03 also provided a detailed comparison of the dynamical properties of supercellular mesocyclones and mesovortices. Specifically, WT03 showed that, in stark contrast to supercellular mesocyclones, bow-echo mesovortices were distinctly a low-level feature that were not associated with the upward dynamic vertical pressure gradient forcing inherent in a pre-existing deep rotating updraft. Moreover, owing to the lack of dynamic updraft forcing, mesovortices do not exhibit significant off-hodograph propagation implying that streamwise vorticity is less important in their generation making the concept of storm-relative environmental helicity somewhat irrelevant in their prediction. WT03 also explained that low-level rotation maximized at the ground implied a downward vertical pressure gradient force which TW03 showed acts to fracture convective lines causing the QLCS to becoming segmented (Fig. 6a).

TW03 analyzed the results of WT03 and found that the strongest surface winds in the simulated MCSs were associated with mesovortices. TW03 ruled out downbursts for the intense winds because they noted the simulated intense winds descend fairly slowly from aloft. Instead, TW03 concluded that damaging winds were driven by the horizontal pressure gradient force associated with pressure deficits in the mesovortices. As such, parcels were initially accelerated by the cold pool and then dramatically accelerated by the pressure drop associated with the mesovortex (see the gray stippled region in Fig. 6a). This led to the strongest winds occurring in conjunction with the mesovortices.

Atkins and St. Laurent (2009a) also examined the relationship of mesovortices to the strength of the low-level shear. As in TW03, they found that mesovortices were strongest for moderate-to-strong low-

level shear. They also attributed this tendency to the fact that stronger low-level shear favored deeper, more upright updrafts that enhanced vorticity stretching and longevity of the simulated mesovortices. Unlike TW03, Atkins and St. Laurent (2009a) determined that the intense surface winds associated with mesovortices were the result of the linear superposition of the descending rear-inflow jet and the flow associated with the mesovortex (Fig. 6b). This result is in agreement with the flow decomposition presented in Wakimoto et al. (2006b).

Noting that previous modeling studies of mesovortices all were performed with homogeneous initial conditions but observational studies (e.g., Przbylinski et al. 2000) had suggested that mesoscale heterogeneity impacted the development of mesovortices, Wheatley and Trapp (2008) investigated the impact of mesoscale heterogeneity on mesovortices. Specifically, through numerical simulations of real cases that included heterogeneous environmental flows, Wheatley and Trapp (2008) concluded that environmental heterogeneity does not play a direct role in mesovortex genesis but could substantially impact mesovortex intensity. More specifically, meso-γ-scale heterogeneity (e.g., a convective gust front from a storm external to the MCS) was found to enhance vorticity stretching and thus lead to mesovortex intensification. On the meso-β-scale, a frontal boundary altered the environmental shear such that updrafts were stronger on the cool side of the frontal boundary, leading to more intense mesovortices there when compared to the warm side of the frontal boundary.

While the observation studies discussed in section 2.1 noted a correspondence between mesovortices and tornadoes, the dynamical relationship between the phenomena has been relatively unexplored in the literature. To the author's knowledge, only Schenkman et al. (2012) has simulated mesovortices with sufficient resolution to capture tornado-like phenomena. Their study simulated a long-lived, tornadic mesovortex with 100-m model grid spacing. Fig. 7 presents their schematic depiction of tornadogenesis in the simulated event. In this schematic, a tornado-like vortex[2] develops within the mesovortex as vorticity is concentrated by low-level convergence associated with an intense low-level updraft on the west side of the mesovortex. Interestingly, this low-level updraft was determined to be the upward branch of a strong horizontal rotor circulation. The vorticity for the rotor was found to be generated by surface drag in the low-level inflow to the mesovortex. It is unknown if this type of rotor circulation is a common occurrence with tornadic mesovortices. More simulations and detailed observational studies are required to explore the relationship between mesovortices and tornadoes.

3. Mesovortex genesis

Now that the relationship between mesovortices, damaging winds, and tornadoes has been reviewed, we turn our attention to the processes behind mesovortex-genesis. With one exception (Wakimoto et al. 2006b), studies of mesovortex-genesis have been based upon numerically simulated convective systems. Several distinct conceptual models have emerged for mesovortex formation. As of this review, there is no reconciliation or agreement about what conceptual model is more generally correct or applicable.

3.1 Downward vortex line tilting – The Trapp and Weisman model

As discussed above, TW03 and WT03 examined quasi-idealized simulations of MCSs over a broad range of environmental shear profiles. During the early stage of the simulated MCS, the mesovortices began as vorticity couplets immediately behind the system gust front, with the cyclonic (anticyclonic) member on the south (north) side of a rainy downdraft. As such, TW03 surmise that these mesovortices are generated via the downward tilting of baroclinically generated vorticity by a localized downdraft associated with a rainwater maximum (Fig. 8a). During the mature stage of the MCS, TW03 found that

[2] Schenkman et al. 2012 call the vortex 'tornado-like' because their simulation did not have adequate resolution to fully resolve the tornado-scale processes associated with the strong sub-mesovortex-scale vortex.

vortex couplets were formed via tilting of horizontal vorticity associated with vertical shear underneath the RIJ. The downdraft responsible for tilting in the mature stage was broader and located several kilometers to the rear of convective gust front. Interestingly, in both the early and mature cases, the symmetry of the vorticity couplet is broken in experiments that include Coriolis forcing. In those experiments, the cyclonic vorticity becomes dominant, developing into a strong, long-lived mesovortex. In experiments that do not include Coriolis forcing, neither the cyclonic nor anti-cyclonic vortex become strong. As such, TW03 conclude that Coriolis forcing is critical in the development of intense mesovortices.

Wakimoto et al. (2006b) examined the genesis of mesovortices via an airborne dual-Doppler radar analysis. They found that vortex couplets developed with the same orientation (i.e., the anti-cyclonic vortex was north of the cyclonic vortex) to the simulation of TW03. However, Wakimoto et al. (2006b) found that the vorticity couplets formed in an area devoid of precipitation which led them to conclude that rainy downdrafts could not be leading to the depression of baroclinically generated vortex lines. Instead, Wakimoto et al. (2006b) determined that mechanically forced, compensating downdrafts on the edge of developing convective storms were responsible for the downward-tilted cold pool baroclinic vortex lines (Fig. 8b). They also note that rainy downdrafts do not develop until the cell is well behind the gust front precluding the scenario envisioned in TW03 from occurring.

3.2 Upward vortex line tilting

Like WT03 and TW03, Atkins and St. Laurent (2009b; hereafter ASL09b) also studied quasi-idealized simulations of MCSs. ASL09b studied the genesis of mesovortices in their simulations and found substantial differences when compared to TW03 and Wakimoto et al. (2006b). Specifically, while vorticity couplets developed in ASL09b, the cyclonic member formed to the north of the anti-cyclonic member. A vortex arch (e.g., Markowski et al. 2008; Straka et al. 2007) connected the cyclonic and anti-cyclonic areas of vorticity. ASL09b suggest that a localized outflow maximum behind the system gust front led to a gust front bulge. Enhanced convergence associated with this gust front bulge caused the development of a localized enhancement in the updraft which arched crosswise baroclinically-generated vortex lines and led to the vorticity couplets in the simulation (Fig. 9a). As in TW03, the cyclonic member of the couplet was favored while the anti-cyclonic member weakened (the simulations in ASL09b all included Coriolis forcing).

ASL09b also found cyclonic-only mesovortices that developed in their simulations. These vortices did not form as part of a vortex-couplet, and instead developed as parcels descended while acquiring baroclinically generated streamwise vorticity (Fig. 9b). This is a similar mechanism to that proposed for low-level mesocyclone formation by Rotunno and Klemp (1985) and Davies-Jones and Brooks (1993). The cyclonic-only mesovortex development generally occurred very early in the simulation and then again late in the simulation once a well-defined rear-inflow jet developed. ASL09b attempt to reconcile the differences in mesovortex-formation conceptual models by simulating the same case studied in Wakiomto et al (2006b) but found that upward tilting of vortex lines was responsible for the generation of mesovortex couplets in their simulation. Wheatley and Trapp (2008) also simulated the case studied in Wakimoto et al. (2006b) and found downward tilting of vortex lines led to the formation of vortex couplets (Fig. 10). As such, reconciling the differences in the ASL09b and TW03 conceptual models is not possible without a large degree of speculation. Instead, we note that both models implicate the tilting of crosswise baroclinically generated vorticity to form vortex couplets. It is also worth noting that both conceptual models for mesovortex genesis conclude that shearing instability is not important in the generation of mesovortices. Earlier observational studies had speculated that shearing instability may play a role in the development of mesovortices (e.g., Przybylinski 1995, Funk et al. 1999, Trapp et al. 1999). These numerical studies do not support that assertion. However, Wheatley and Trapp (2008) found that in a

strongly-forced, cool-season QLCS, system-scale tilting of extremely large environmental vorticity led to the development of a vortex sheet. Shearing instability in this vortex sheet was implicated in the development of mesovortices in this case.

3.3 The role of surface drag

Further complicating the conceptualization of the formation of mesovortices, a recent study by Xu et al. (2015a) has implicated the importance of surface drag in the generation of mesovortices. Both TW03 and ASL09b neglected surface drag in their quasi-idealized simulations of mesovortices. In contrast, Xu et al. (2015b) simulated the 8 May 2009 super-derecho (e.g., Coniglio et al. 2010; Weisman et al. 2013) at 800-m grid spacing, starting from an initial condition that assimilated all available observations. This real data simulation employed a full physics package that included a surface drag parameterization. Through circulation (e.g., Rotunno and Klemp 1985) and trajectory analysis, Xu et al. (2015b) found that surface drag played a significant role in generating vorticity that fed into the developing mesovortices (Fig. 11). The simulation examined in Schenkman et al. (2012) also showed that surface drag played a role in mesovortex dynamics, but in their study baroclinic vorticity generation and subsequent arching (as in ASL09b) were found to be directly responsible for mesovortex rotation. Owing to the lack of more simulation studies that include surface drag, it is not possible at this time to assess the generality of the conclusions presented in Xu et al. (2015b). Additionally, the fact that free-slip simulations (e.g., TW03, ASL09b) produced mesovortices implies that surface drag is not necessary to *simulate* mesovortex genesis. It is also worth noting that rather than explicitly calculating the contribution of surface drag to circulation and vorticity budgets, Xu et al. (2015b) treat frictionally generated circulation and vorticity as the residual in their calculations. More simulations that include surface drag and explicitly calculate its contribution to vorticity and circulation in mesovortices are required to determine if frictionally generated vorticity always plays an important role in mesovortex genesis. A recent real-data simulation study by Schenkman et al. (2014) also pointed out the importance of frictionally generated horizontal vorticity as a source of rotation for tornadogenesis within a supercell storm, so the potential importance of frictional vorticity generation for the intensification of low-level vortices is definitely worth investigating.

4. Forecasting mesovortices

Despite the differences in mesovortex genesis conceptualizations, case studies of convection-resolving numerical simulations show promising results for the accurate prediction of bow-echoes and associated mesovortices (Schenkman et al. 2011a, b; Schenkman et al. 2012; Snook et al. 2011; Snook et al. 2012; Snook et al. 2015; Weisman et al. 2013; Wheatley and Trapp 2008; Wheatley et al. 2012; Xu et al. 2015a, b). In this section, two such case studies are reviewed in-depth: The 8-9 May 2007 Oklahoma tornadic convective system (e.g., Schenkman et al. 2011a,b) and the 8 May 2009 'super-derecho' (Weisman et al. 2013, Xu et al. 2015a,b).

4.1 The 8-9 May 2007 tornadic convective system.

On 8 May 2007, a large MCS formed over eastern NM and west TX. The MCS persisted throughout the day and upon entering west-central Oklahoma that night began producing tornadic and non-tornadic mesovortices. The mesovortices were generally located in the comma-echo portion of the MCS (e.g., Fujita 1978; Pfost and Gerard 1997). Tornadic mesovortices were found to be longer-lived than non-tornadic mesovortices (Schenkman et al. 2011b) in agreement with Atkins et al. (2004) and Atkins et al. (2005). Schenkman et al. (2011a,b) used the Advanced Regional Prediction system (ARPS; e.g., Xue et al. 2003) 3DVAR with a cloud analysis package (e.g., Hu et al. 2006) to assimilate multiple sources of data from this case. Assimilated data included conventional surface and upper air observations, WSR-88D reflectivity and velocity data, and radar data from the experimental Collaborative and Adaptive Sensing of the Atmosphere's IP-I network (CASA; e.g., McLaughlin et al. 2009). The CASA IP-I network was

designed to fill the gap in low-level radar coverage (< 1 km AGL) in southwest Oklahoma between the Twin Lakes (KTLX)and Frederick (KFDR) WSR-88Ds.

Schenkman et al. (2011a) found that accurate short term forecasts (up to 3 h) of the overall convective system and line-end vortex could be produced by the ARPS model when radar data were assimilated, using 2-km grid spacing (Fig. 12). The assimilation of CASA data had a small positive impact on the forecast accuracy of the line-end vortex track in Schenkman et al. (2011a). Encouraged by the results of the system-scale simulation, Schenkman et al. (2011b) assimilated the same data sources at 400-m grid spacing with the goal of investigating the impacts on the forecasts of mesovortices in the case. At this resolution, low-level radial wind data assimilation from CASA had a substantial impact on the analysis and forecast of the sub-system scale features. Specifically, low-level wind data assimilation led to a more accurate depiction of the near-storm low-level shear and gust front position during the analysis period (not shown). During the forecast period experiments that assimilated low-level winds produced much more accurate 1-2 h forecasts of the location, intensity, and duration of one of the observed long-lived mesovortices associated with the QLCS (Fig. 13) . Experiments that did not assimilate low-level wind data produced numerous weak mesovortices that developed too early in the simulation and rapidly dissipated (Fig. 13e).

Schenkman et al. (2012) further nested a grid with a 100-m spacing within one of the 400-m grid spacing forecasts from Schenkman et al. (2011b). As discussed in section 2, this simulation produced a weak tornado-like vortex in association with the long-lived mesovortex forecasted. In the observed case, this long-lived mesovortex also produced a weak tornado in a similar location as in the simulated experiment. Though the tornado-like vortex occurred 20 min too early in the 100-m forecast, the similarities to the evolution of the observed tornadic mesovortex are encouraging for providing significantly enhanced lead-time for mesovortex tornadoes. This enhanced lead time is necessary for the National Weather Service's proposed shift to a warn-on-forecast paradigm, where warnings for hazards are issued based on high-resolution numerical forecasts rather than upon detection (e.g., Stensrud et al. 2009; Stensrud et al. 2012).

Snook et al. (2011, 2012, 2015) also examined the same 8-9 May 2007 MCS but used the ensemble Kalman filter (EnKF) (instead of 3DVAR) data assimilation system of Tong and Xue (2005) and Xue et al. (2006), and produced probabilistic instead of deterministic forecasts. Like Schenkman et al. (2011a,b), Snook et al. (2012, 2015) obtained accurate forecasts of track and timing of the line-end vortex and an associated long-lived mesovortex. They also demonstrated potential skills in probabilistic forecasting of tornado-like vortices within a high-resolution numerical model.

Taken as a whole, the results of this multi-scale case study suggest that it may be possible to accurately forecast the development of strong, long-lived mesovortices with up to 2 hours of lead time given adequate low-level observations. This result is reinforced by the fact that accurate forecasts were produced using two distinct data assimilation methods as well as in both a deterministic and probabilistic framework.

4.2 The 8 May 2009 Super Derecho

On 8 May 2009, an unusually intense MCS produced widespread wind damage and multiple tornadoes across Kansas, southern Missouri, and southern Illinois (Fig. 14a). Convective initiation occurred along the eastern slope of the Rocky Mountains in Colorado. The system intensified as it encountered unusually strong and deep low-level jet in Kansas and Missouri (Coniglio et al. 2010). As the MCS matured a very intense warm-core mesolow formed at the northern tip of the bow-echo. Weisman et al. (2013) examined a real-time 3-km grid spacing simulation of this system produced with Advanced Research core of the Weather Research Forecasting model (WRF-ARW; Skamarock and Klemp 2008). This simulation

accurately captured the development of many of the key features of the observed event, including the mesolow, up to 24 h in advance (Fig. 14b). However, Weisman et al. (2013) note that while many mesovortices were observed in the actual event, they were not present in the WRF-ARW simulation likely owing to insufficient resolution.

Xu et al. (2015b) used Doppler radar observations to examine the mesovortices observed during the mature phase of the 8 May 2009 super derecho in more detail. They identify 9 mesovortices (Fig. 14c), 5 of which were tornadic. All tornadic mesovortices were located to the north of the bow echo apex. Xu et al. (2015b) also generated and examined a 0.8-km grid interval simulation of the super derecho, that was nested within a 4-km CONUS-domain realtime forecast from the Center for Analysis and Prediction of Storms (CAPS)_storm-scale ensemble forecast (SSEF) runs (Xue et al. 2009). The simulation in Xu et al. (2015a) also produced 9 mesovortices (Fig. 14d) during the period they examined (that spanned from 1400 to 1640 UTC with the initial condition being at 0000 UTC). Though there is not a one-to-one correspondence between simulated and observed mesovortices, the simulated mesovortices from Xu et al. (2015b) generally follow a similar path and are in a similar MCS-relative location as the observed mesovortices (Fig. 14c,d). Analysis of these mesovortices show that high winds were generally associated with the mesovortices near the bow echo apex. In agreement with ASL09a and Wakimoto et al (2006b), these high winds were caused by the superposition of the rear-inflow jet and the mesovortex flow.

The reasonably skillful mesoscale and storm-scale forecasts of the 8 May 2009 super derecho present a possible blueprint for operational forecasting of bow-echo mesovortices in a warn on forecast context. More specifically, a convection-resolving simulation of a bow-echo could be used to initialize a higher-resolution nested simulation capable of resolving mesovortices. While a one-to-one correspondence of model forecasted and observed mesovortices is highly unlikely beyond the typical life cycle of mesovortices, these mesovortex-resolving simulations could be used to alert operational forecasters to the potential for long-lived mesovortices, and thus, damaging winds and tornadoes up to 24 hours in advance of a severe weather event. When an ensemble of such forecasts is produced, probabilistic information could also be provided.

5. A look ahead

Great strides have been made in the understanding of mesovortices and their association with high winds and tornadoes in QLCSs. Interestingly, however, the dynamics behind mesovortex generation remains an open research problem. At least five hypotheses exist that explain mesovortex genesis. In the first three hypotheses (i-iii), vortex couplets are formed as storm-generated (baroclinic) vortex lines are either depressed downward by (i) rainy downdrafts (e.g., TW03), or (ii) mechanically forced downdrafts (Wakimoto et al. 2006b), or are arched upward by (iii) a localized updraft enhancement (ASL09b, Schenkman et al. 2012) . In contrast, the other two hypothesis (iv-v) explain the development of cyclonic-only mesovortices via the tilting of (iv) baroclinic vorticity as parcels descend parallel to the convective gust front (ASL09b) or (v) frictionally generated vorticity as parcels ascend at the gust front (Xu et al. 2015b). Future work should focus on obtaining high-quality observational data sets of MCSs that spawn mesovortices in order to initialize high-resolution model simulations through advanced data assimilation methods (e.g., Schenkman et al. 2011a,b; Snook et al 2012,2015). Vorticity calculations along trajectories combined with circulation analyses should provide the necessary evidence to determine what mesovortex genesis mechanism is occurring in the simulations. Inclusion of a surface drag parameterization is imperative in these simulations in order to assess the validity of the mesovortex genesis mechanism proposed by Xu et al. (2015b). It is also possible that the mesovortex genesis mechanism will vary depending on model parameters. For example, as discussed above, ASL09b used a different configuration of the WRF-ARW to simulate the same case as Wheatley et al. (2008) and found a different mesovortex

genesis mechanism. An idealized model parameter study, perhaps including different forecast models, may be necessary to understand the sensitivity of the conclusions on the model and model configurations.

The dynamical relationship between mesovortices and tornadoes is another area with many opportunities for future research. While it has been shown that tornadic mesovortices tend to be longer-lived and deeper than non-tornadic mesovortices, the root causes behind this tendency remain relatively unexplored. Specifically, it is unknown why some mesovortices are stronger and longer-lived than other mesovortices within the same system. It is encouraging that case studies of these mesovortex-producing systems have shown promise in forecasting the development of long-lived mesovortices. With the continued increase in computational power, as well as advances in data assimilation techniques and improvement in the accuracy of numerical models, it should be possible to produce more simulations that capture tornado-like processes. Assuming the simulations can accurately portray tornado-like vortices, analysis of these simulations should allow researchers to gain a more fundamental understanding of the dynamical relationship between mesovortices and the tornadoes they spawn. Increased understanding, along with accurate forecast models, may give forecasters the information they need to better anticipate the development of tornadoes in association with mesovortices thus reducing false-alarms and increasing lead-time for tornado warnings in these scenarios.

Acknowledgements: This work was primarily supported by NSF grant AGS-0802888. Additional support was provided by the National 973 Fundamental Research Program of China (2013CB430103), and NSF grants AGS-1046171 and AGS-1261776.

References

Atkins, N. T., J. M. Arnott, R. W. Przybylinski, R. A. Wolf, and B. D. Ketcham, 2004: Vortex Structure and Evolution within Bow Echoes. Part I: Single-Doppler and Damage Analysis of the 29 June 1998 Derecho. *Mon. Wea. Rev.*, **132,** 2224-2242.

Atkins, N. T., C. S. Bouchard, R. W. Przybylinski, R. J. Trapp, and G. Schmocker, 2005: Damaging Surface Wind Mechanisms within the 10 June 2003 Saint Louis Bow Echo during BAMEX. *Mon. Wea. Rev.*, **133,** 2275-2296.

Atkins, N. T. and M. St. Laurent, 2009a: Bow echo mesovortices. Part I: Processes that influence their damaging potential. *Mon. Wea. Rev.*, **137,** 1497-1513.

Atkins, N. T. and M. St. Laurent, 2009b: Bow echo mesovortices. Part II: Their genesis. *Mon. Wea. Rev.*, **137,** 1514-1532.

Burgess, D. W. and B. F. Smull, 1990: Doppler radar observations of a bow echo associated with a long-track severe windstorm. *16th Conf. on Severe Local Storms*, Kananaskis Park, AB, Canada, Amer. Meteor. Soc., 203-208.

Coniglio, M. C., S. F. Corfidi, and J. S. Kain, 2010: Environment and Early Evolution of the 8 May 2009 Derecho-Producing Convective System. *Mon. Wea. Rev.*, **139,** 1083-1102.

Davies-Jones, R. P. and H. Brooks, 1993: Mesocyclogenesis from a theoretical perspective. *The Tornado: Its Structure, Dynamics, Prediction, and Hazards*, C. R. Church, Ed., Amer. Geophys. Union Press, 105-114.

Davis, C., N. Atkins, D. Bartels, L. Bosart, M. Coniglio, G. Bryan, W. Cotton, D. Dowell, B. Jewett, R. Johns, D. Jorgensen, J. Knievel, K. Knupp, W.-C. Lee, G. Mcfarquhar, J. Moore, R. Przybylinski, R. Rauber, B. Smull, R. Trapp, S. Trier, R. Wakimoto, M. Weisman, and C. Ziegler, 2004: The Bow Echo and MCV Experiment: Observations and opportunities. *Bull. Amer. Meteor. Soc.*, **85,** 1075-1093.

Forbes, G. S. and R. M. Wakimoto, 1983: A concentrated outbreak of tornadoes, downbursts and microbursts, and implications regarding vortex classification. *Mon. Wea. Rev.*, **111,** 220-235.

Fujita, T. T., 1978: Manual of downburst identification for project Nimrod. Satellite and Mesometeorology Res. Pap. 156. Dept. of Geophysical Science, University of Chicago, 104pp [NTISPB-286048].

Fujita, T. T., 1979: Objective, operation, and results of Project NIMROD. *11th Conf. on Severe Local Storms*, Kansas City, MO, Amer. Meteor. Soc., 259-266.

Fujita, T. T., 1981: Tornadoes and downbursts in the context of generalized planetary scales. *J. Atmos. Sci.*, **38,** 1511-1534.

Fujita, T. T. and R. M. Wakimoto, 1981: Five scales of airflow associated with a series of downbursts of 16 July 1980. *Mon. Wea. Rev.*, **109,** 1438-1456.

Funk, T., K. Darmofal, J. Kirkpatrick, V. DeWald, R. Przbylinski, G. Schmocker, and Y.-J. Lin, 1999: Storm reflectivity and mesocyclone evolution assocaited with the 15 April 1994 squall line of Kentucky and southern Indiana. *Wea. Forecasting*, **14,** 976-993.

Houze, R. A., Jr., S. A. Rutledge, M. I. Biggerstaff, and B. F. Smull, 1989: Interpretation of Doppler weather radar displays of midlatitude mesoscale convective systems. *Bull. Amer. Meteor. Soc.*, **70,** 607-619.

Hu, M., M. Xue, and K. Brewster, 2006: 3DVAR and cloud analysis with WSR-88D level-II data for the prediction of Fort Worth tornadic thunderstorms. Part I: Cloud analysis and its impact. *Mon. Wea. Rev.*, **134,** 675-698.

Johnston, E. C., 1981: Mesoscale vorticity centers induced by mesoscale convective complexes, M. S., Dept. of Meteor., University of Wisconsin, 54 pp.

Jorgensen, D. P. and B. F. Smull, 1993: Mesovortex circulations seen by air-borne Doppler radar within a bow-echo mesoscale convective system. *Bull. Amer. Meteor. Soc.*, **74,** 2146-2157.

Klemp, J. B. and R. B. Wilhelmson, 1978: The simulation of three-dimensional convective storm dynamics. *J. Atmos. Sci.*, **35,** 1070-1096.

Klimowski, B. A., 1994: Initiation and development of rear inflow within the 28-29 June 1989 North Dakota mesoconvective system. *Mon. Weal Rev.*, **122,** 765-779.

Markowski, P., E. Rasmussen, J. Straka, R. Davies-Jones, Y. Richardson, and R. J. Trapp, 2008: Vortex lines within low-level mesocyclones obtained from pseudo-dual-doppler radar observations. *Mon Weather Rev*, **136,** 3513-3535.

McLaughlin, D., D. Pepyne, V. Chandrasekar, B. Philips, J. Kurose, M. Zink, K. Droegemeier, S. Cruz-Pol, F. Junyent, J. Brotzge, D. Westbrook, N. Bharadwaj, Y. Wang, E. Lyons, K. Hondl, Y. Liu, E. Knapp, M. Xue, A. Hopf, K. Kloesel, A. DeFonzo, P. Kollias, K. Brewster, R. Contreras, B. Dolan, T. Djaferis, E. Insanic, S. Frasier, and F. Carr, 2009: Short-wavelength technology and the potential for distributed networks of small radar systems. *Bull. Amer. Meteor. Soc.*, **90,** 1797-1817.

Menard, R. D. and J. M. Fritsch, 1989: A mesoscale convective complex-generated inertially stable warm core vortex. *Mon. Wea. Rev.*, **117,** 1237-1260.

Orlanski, I., 1975: A rational subdivision of scales for atmospheric processes. *Bull. Amer. Meteor. Soc.*, **56,** 527-530.

Pfost, R. L. and A. E. Gerard, 1997: "Bookend vortex"–induced tornadoes along the Natchez Trace. *Wea. Forecasting*, **12,** 572-580.

Przbylinski, R., G. Schmocker, and Y.-J. Lin, 2000: A study of storm and vortex morphology during the "intensifying stage" of severe wind mesoscale convective systems. *20th Conf. on Severe Local Storms*, Amer. Meteor. Soc., 173-176.

Przybylinski, R. W., 1995: The bow echo. Observations, numerical simulations, and severe weather detection methods. *Wea. Forecasting*, **10,** 203-218.

Rotunno, R. and J. B. Klemp, 1985: On the rotation and propagation of simulated supercell thunderstorms. *J. Atmos. Sci.*, **42,** 271-292.

Schenkman, A., M. Xue, A. Shapiro, K. Brewster, and J. Gao, 2011a: The analysis and prediction of the 8-9 May 2007 Oklahoma tornadic mesoscale convective system by assimilating WSR-88D and CASA radar data using 3DVAR. *Mon. Wea. Rev.*, **139,** 224-246.

Schenkman, A., M. Xue, A. Shapiro, K. Brewster, and J. Gao, 2011b: Impact of CASA radar and Oklahoma mesonet data assimilation on the analysis and prediction of tornadic mesovortices in a MCS. *Mon. Wea. Rev.*, **139,** 3422-3445.

Schenkman, A., M. Xue, and A. Shapiro, 2012: Tornadogenesis in a simulated mesovortex within a mesoscale convective system. *J. Atmos. Sci.*, **69,** 3372-3390.

Schenkman, A., M. Xue, and M. Hu, 2014: Tornadogenesis within numerically simulated 8 May 2003 Oklahoma City tornadic supercell storm. *J. Atmos. Sci.*, **71,** 130-154.

Skamarock, W. C., M. L. Weisman, and J. B. Klemp, 1994: Three-dimensional evolution of simulated long-lived squall lines. *J. Atmos. Sci.*, **51,** 2563-2584.

Skamarock, W. C. and J. B. Klemp, 2008: A time-split nonhydrostatic atmospheric model for weather research and forecasting applications. *J. Comput. Phys.*, **227,** 3465-3485.

Smull, B. F. and R. A. Houze, Jr., 1987: Rear inflow in squall lines with trailing stratiform precipitation. *Mon. Wea. Rev.*, **115,** 2869-2889.

Snook, N., M. Xue, and J. Jung, 2011: Analysis of a tornadic meoscale convective vortex based on ensemble Kalman filter assimilation of CASA X-band and WSR-88D radar data. *Mon. Wea. Rev.*, **139,** 3446-3468.

Snook, N., M. Xue, and Y. Jung, 2012: Ensemble probabilistic forecasts of a tornadic mesoscale convective system from ensemble Kalman filter analyses using WSR-88D and CASA radar data. *Mon. Wea. Rev.*, **140,** 2126-2146.

Snook, N., M. Xue, and Y. Jung, 2015: Multiscale EnKF assimilation of radar and conventional observations and ensemble forecasting for a tornadic mesoscale convective system. *Mon. Wea. Rev.*, **143,** 1035-1057.

Stensrud, D. J., M. Xue, L. J. Wicker, K. E. Kelleher, M. P. Foster, J. T. Schaefer, R. S. Schneider, S. G. Benjamin, S. S. Weygandt, J. T. Ferree, and J. P. Tuell, 2009: Convective-scale Warn on Forecast System: A Vision for 2020. *Bull. Am. Meteor. Soc.*, **90,** 1487-1499.

Stensrud, D. J., L. J. Wicker, M. Xue, D. Dawson, N. Yussouf, D. Wheatley, T. E. Thompson, N. A. Snook, T. M. Smith, A. D. Schenkman, C. K. Potvin, E. R. Mansell, T. Lei, K. M. Kuhlman, Y. Jung, T. A. Jones, J. Gao, M. C. Coniglio, H. E. Brooks, and K. A. Brewster, 2012: Progress and challenges with Warn-on-Forecast. *Atmos. Res.***,** In press.

Straka, J., E. Rasmussen, R. Davies-Jones, and P. Markowski, 2007: An observational and idealized numerical examination of low-level counter-rotating vortices toward the rear flank of supercells. *Electron. J. Severe Storms Meteor*, **2,** 1-22.

Tong, M. and M. Xue, 2005: Ensemble Kalman filter assimilation of Doppler radar data with a compressible nonhydrostatic model: OSS Experiments. *Mon. Wea. Rev.*, **133,** 1789-1807.

Trapp, R. J., S. A. Tessendorf, E. S. Godfrey, and H. Brooks, 1999: Descending and nondescending tornadic vortex signatures detected by WSR-88Ds. *Wea. Forecasting*, **14,** 625-639.

Trapp, R. J. and M. L. Weisman, 2003: Low-Level mesovortices within squall lines and bow echoes. Part II: Their genesis and implications. *Mon. Wea. Rev.*, **131,** 2804-2823.

Trapp, R. J., S. A. Tessendorf, E. S. Godfrey, and H. E. Brooks, 2005: Tornadoes from squall lines and bow echoes. Part I: Climatological distribution. *Wea. Forecasting*, **20,** 23-34.

Wakimoto, R. M., H. V. Murphey, A. Nester, D. P. Jorgensen, and N. T. Atkins, 2006a: High winds generated by bow echoes. Part I: Overview of the Omaha bow echo 5 July 2003 storm during BAMEX. *Mon. Wea. Rev.*, **134,** 2793-2812.

Wakimoto, R. M., H. V. Murphey, C. A. Davis, and N. T. Atkins, 2006b: High winds generated by bow echoes. Part II: The relationship between the mesovortices and damaging straight-line winds. *Mon. Wea. Rev.*, **134,** 2813-2829.

Weisman, M., C. Evans, and L. Bosart, 2013: The 8 May 2009 superderecho: Analysis of a real-time explicit convective forecast. *Wea. Forecasting*, **28,** 863-892.

Weisman, M. L., 1992: The role of convectively generated rear-inflow jets in the evolution of long-lived mesoconvective systems. *J. Atmos. Sci.*, **49,** 1826-1847.

Weisman, M. L., 1993: The genesis of severe long-lived bow-echoes. *J. Atmos. Sci.*, **50,** 645-670.

Weisman, M. L. and C. A. Davis, 1998: Mechanisms for the generation of mesoscale vortices within quasi-linear convective systems. *J. Atmos. Sci.*, **55,** 2603-2622.

Weisman, M. L. and R. J. Trapp, 2003: Low-Level Mesovortices within Squall Lines and Bow Echoes. Part I: Overview and Dependence on Environmental Shear. *Mon. Wea. Rev.*, **131,** 2779-2803.

Wheatley, D. M., R. J. Trapp, and N. T. Atkins, 2006: Radar and Damage Analysis of Severe Bow Echoes Observed during BAMEX. *Mon. Wea. Rev.*, **134,** 791-806.

Wheatley, D. M. and R. J. Trapp, 2008: The effect of mesoscale heterogeneity on the genesis and structure of mesovortices within quasi-linear convective systems. *Mon. Wea. Rev.*, **136,** 4220–4241.

Wheatley, D. M., D. J. Stensrud, D. Dowell, and N. Yussouf, 2012: Application of a WRF mesoscale data assimilation system to springtime severe weather events 2007-09. *Mon. Wea. Rev.*, **140,** 1539-1557.

Wolf, P. L., 1998: WSR-88D radar depiction of supercell-bow echo interaction: Unexpected evolution of a large,tornadic,comma-shaped supercell of eastern Oklahoma. *Wea. Forecasting*, **13,** 492-504.

Xu, X., M. Xue, and Y. Wang, 2015a: The genesis of mesovortices within a real-data simulation of a bow echo system. *J. Atmos. Sci.*, **72,** 1963-1986.

Xu, X., M. Xue, and Y. Wang, 2015b: Mesovortices within the 8 May 2009 bow echo over central US: Analyses of the characteristics and evolution based on Doppler radar observations and a high-resolution model simulation. . *Mon. Wea. Rev.*, **143,** 2266-2290.

Xue, M., D.-H. Wang, J.-D. Gao, K. Brewster, and K. K. Droegemeier, 2003: The Advanced Regional Prediction System (ARPS), storm-scale numerical weather prediction and data assimilation. *Meteor. Atmos. Phy.*, **82,** 139-170.

Xue, M., M. Tong, and K. K. Droegemeier, 2006: An OSSE framework based on the ensemble square-root Kalman filter for evaluating impact of data from radar networks on thunderstorm analysis and forecast. *J. Atmos. Ocean Tech.*, **23,** 46–66.

Xue, M., F. Kong, K. W. Thomas, J. Gao, Y. Wang, K. Brewster, K. K. Droegemeier, X. Wang, J. Kain, S. Weiss, D. Bright, M. Coniglio, and J. Du, 2009: CAPS realtime multi-model convection-allowing ensemble and 1-km convection-resolving forecasts for the NOAA Hazardous Weather Testbed 2009 Spring Experiment. *23nd Conf. Wea. Anal. Forecasting/19th Conf. Num. Wea. Pred.*, Omaha, NB, Amer. Meteor. Soc., Paper 16A.2.

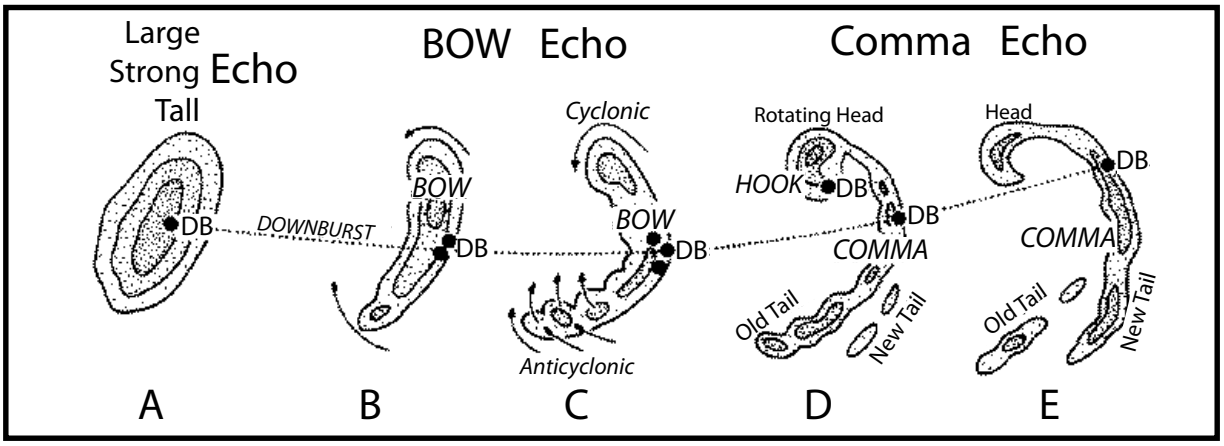

Fig. 1. Radar morphology of bow echoes that produce strong and extensive downbursts, labeled DB. [From Fujita (1978)]

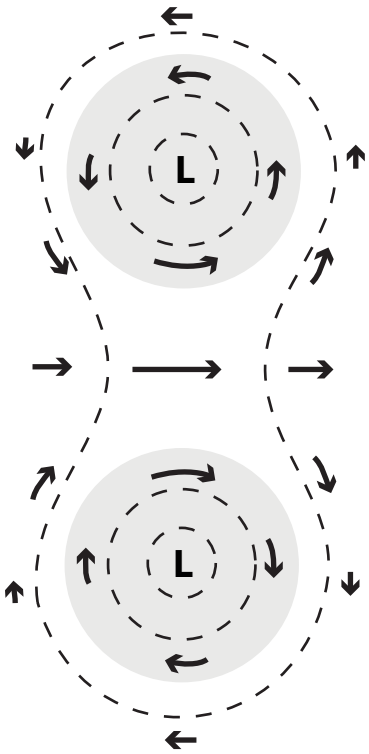

Fig. 2. Schematic representation of an idealized two-dimensional vortex couplet. Strong flow is induced between the vortices. The shading represents regions of constant vorticity. Dashed contours mark the area of a negative pressure perturbation field associated with the flow pattern. The 'L' marks the location of lowest pressure. [Adapted from Weisman (1993)]

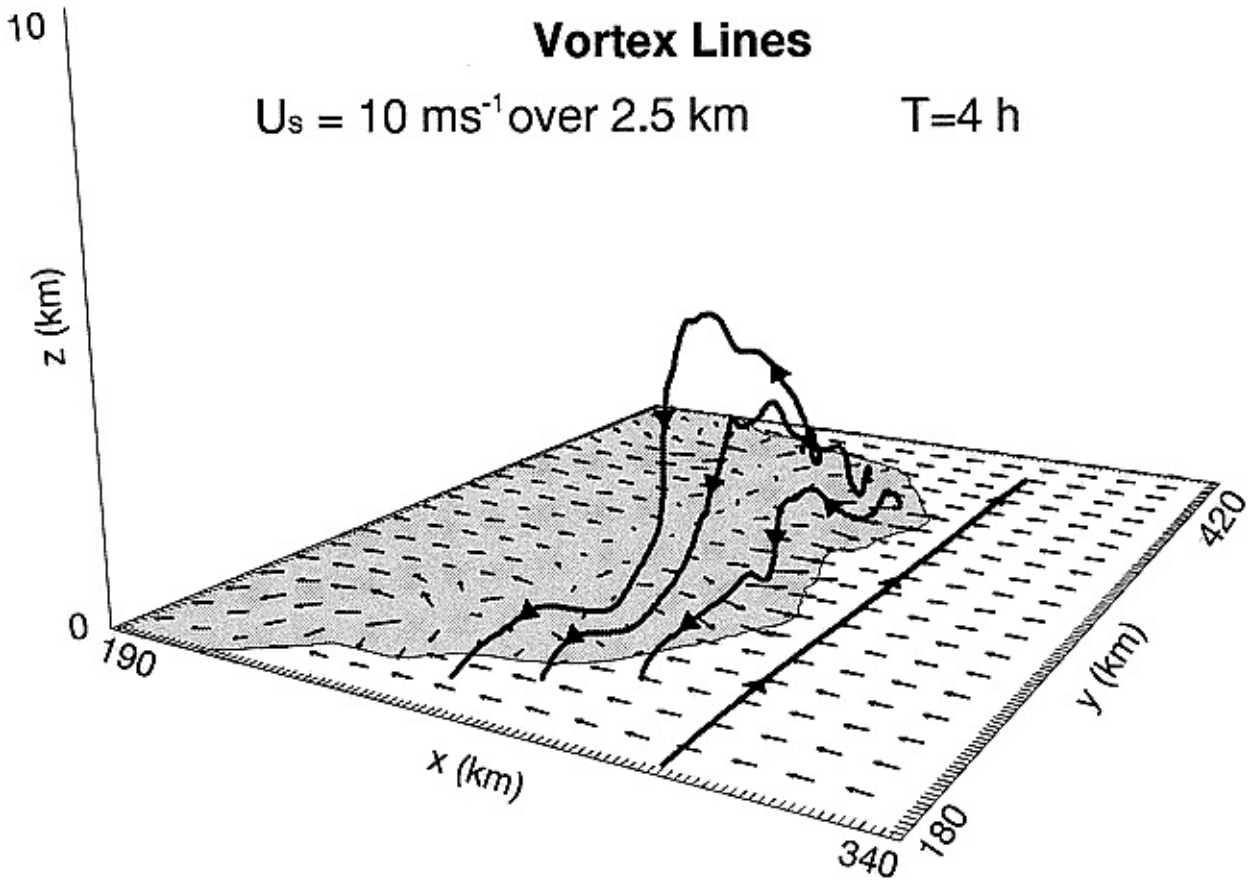

Fig. 3. Three-dimensional depiction of vortex lines (denoted by the thick solid lines) arching over a simulated cold pool (<- 1 K, shaded). Vectors are represent the surface wind flow. [From Weisman and Davis (1998)]

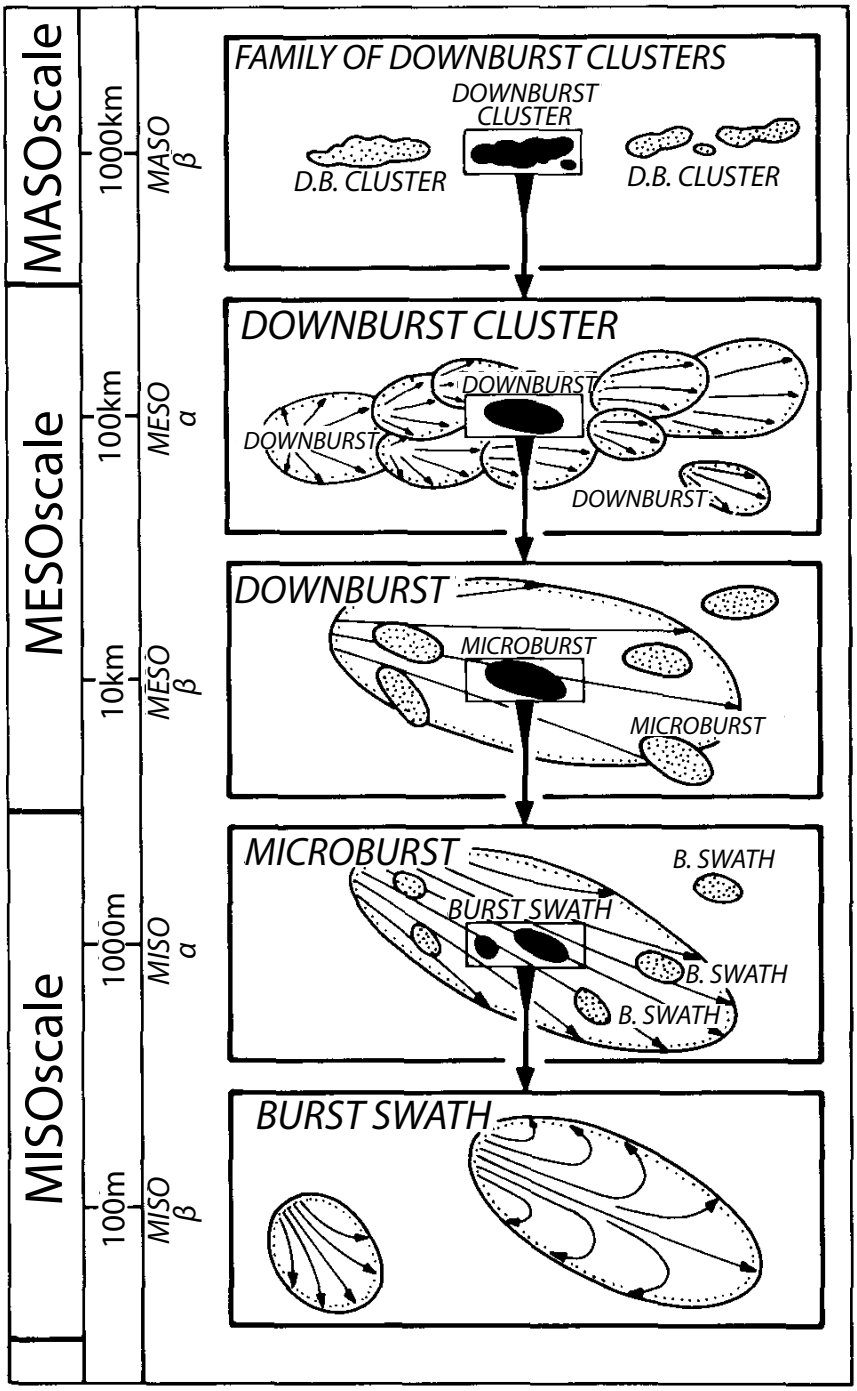

Fig. 4. Five scales of downburst damage patterns identified via detailed post-storm damage surveys. Note that the definition of scales differs from those of Orlanski (1975). [From Fujita and Wakimoto (1981)]

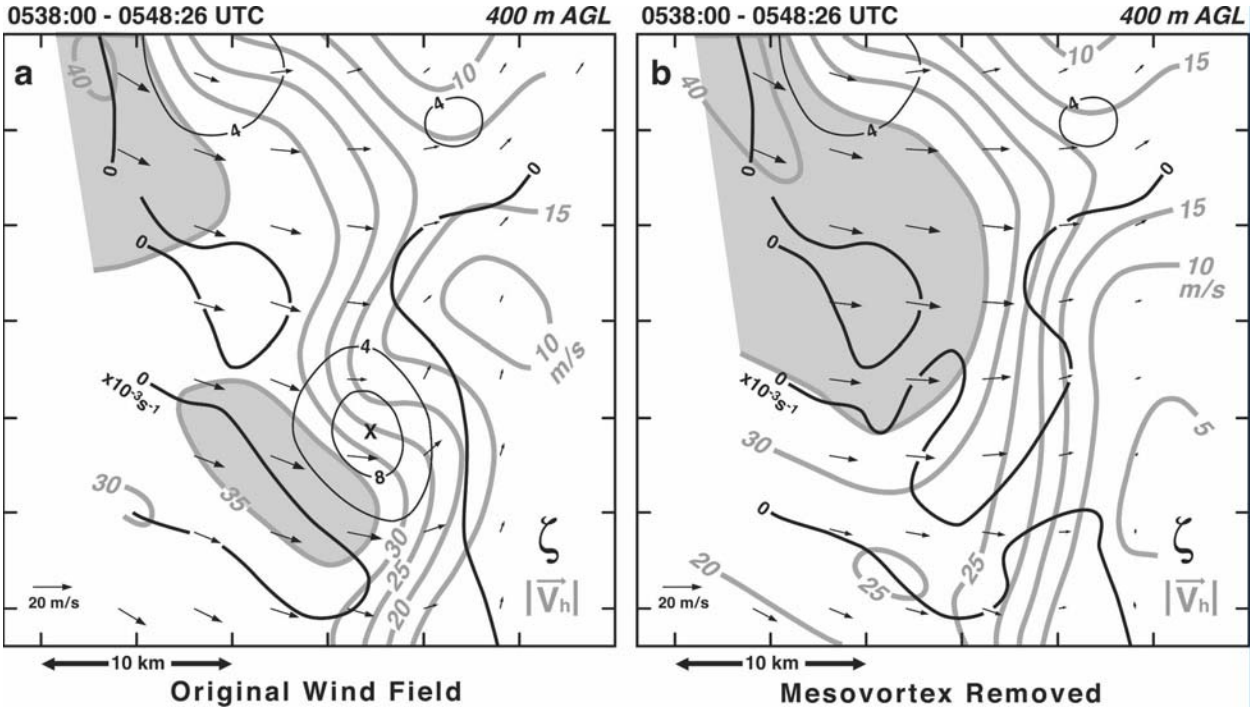

Fig. 5. Doppler wind synthesis at 0538:00-00548:26 UTC 5 July 2003 at 400 m AGL for a mesovortex associated with damaging winds. In (a) the total analyzed wind field is plotted. In (b), the circulation associated with the mesovortex is removed. Wind > 35 m s^{-1} are shaded in gray. Black and gray lines are vertical vorticity and isotachos, respectively. [From Wakimoto et al (2006b)].

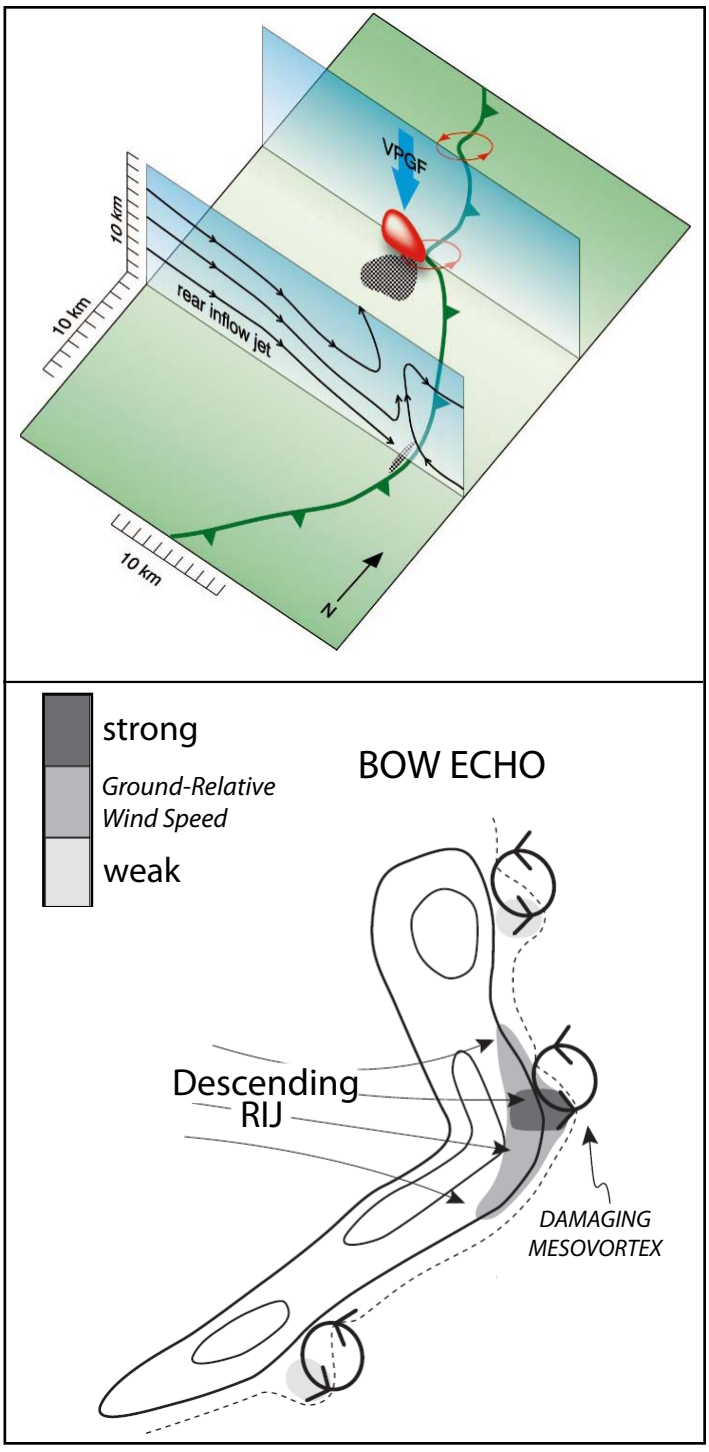

Fig. 6. Two schematic depictions of the relationship between mesovortices and damaging winds in bow echoes. (Top) From Trapp and Weisman (2003), the red circles represent mesovortices, the red blob in the vertical plane represents vertical vorticity. The downward-directed PGF (blue arrow) acts to fracture the updraft of the convective system. The gray stippled area shows severe winds associated with the mesovortex and descending RIJ. (Bottom) From Atkins and St. Laurent (2009a). The dark shading shows where damaging winds are found as a result of the superposition of the RIJ and the mesovortex flow.

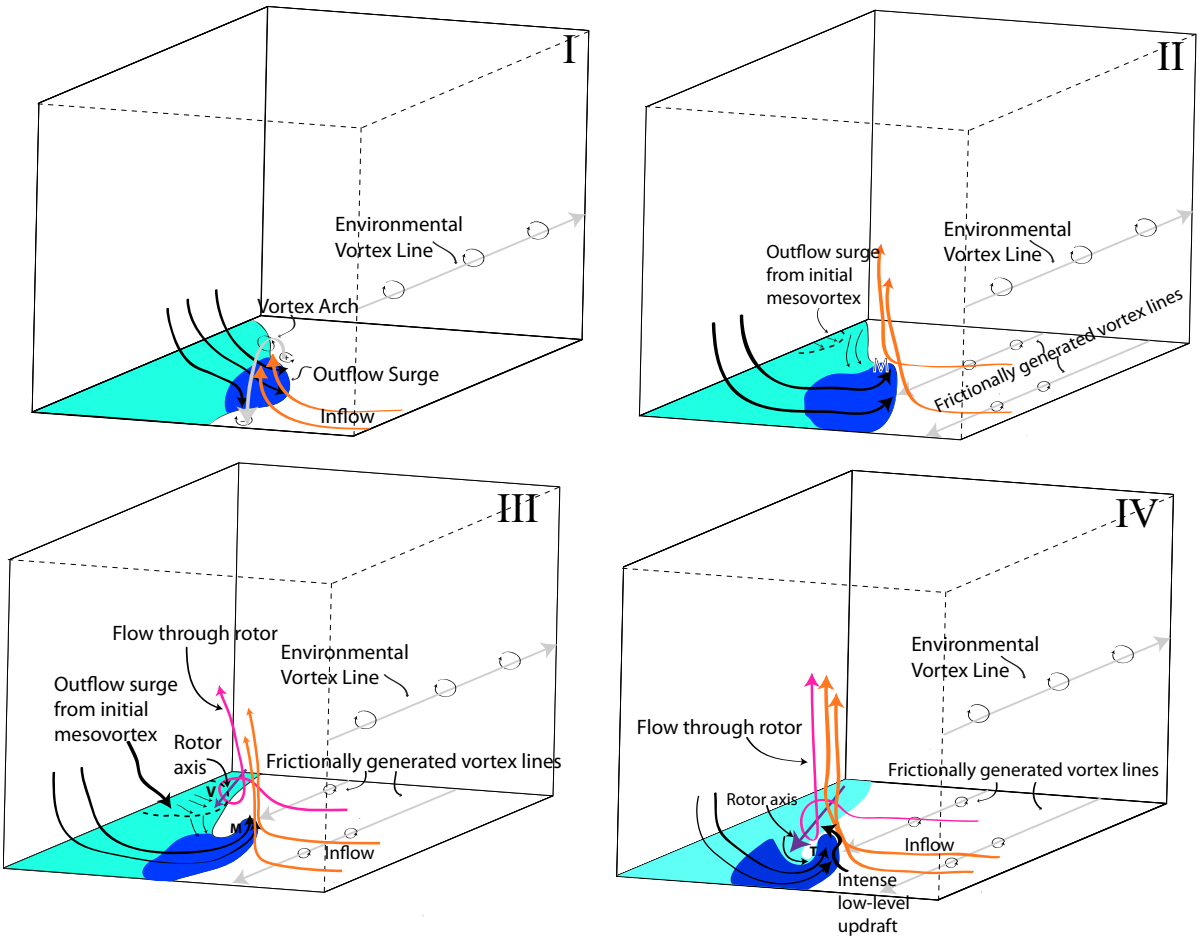

Fig. 7. Schematic of four-stage process leading up to genesis of a tornado-like vortex (TLV) associated with a mesovortex from Schenkman et al. (2012). Vertical vorticity couplet development is depicted in (I). (II) shows the development of a dominant cyclonic mesovortex and associated development of the frictionally-generated horizontal vorticity. (III) Illustrates the development of the rotor. TLV genesis is shown in (IV). The cyan shading represents the cold pool. The dark blue shading represents enhanced cold air within the cold pool bulge. Black arrows represent the surface flow trajectories. The orange arrows represent trajectories which enter the main updraft. The purple arrow in (III) and (IV) marks the horizontal rotor axis. The magenta arrows represent parcel trajectories that enter the rotor. Light gray vectors are idealized vortex lines. The 'M' represents the location of the mesovortex. The dotted curves in (II) and (III) mark the location of the enhanced westerly momentum associated with the dissipation of an mesovortex. The 'v' behind the outflow surge from the initial mesovortex in (III) marks the location of the small area of vertical vorticity moving through the rotor. The 'T' in (IV) marks the location of the TLV.

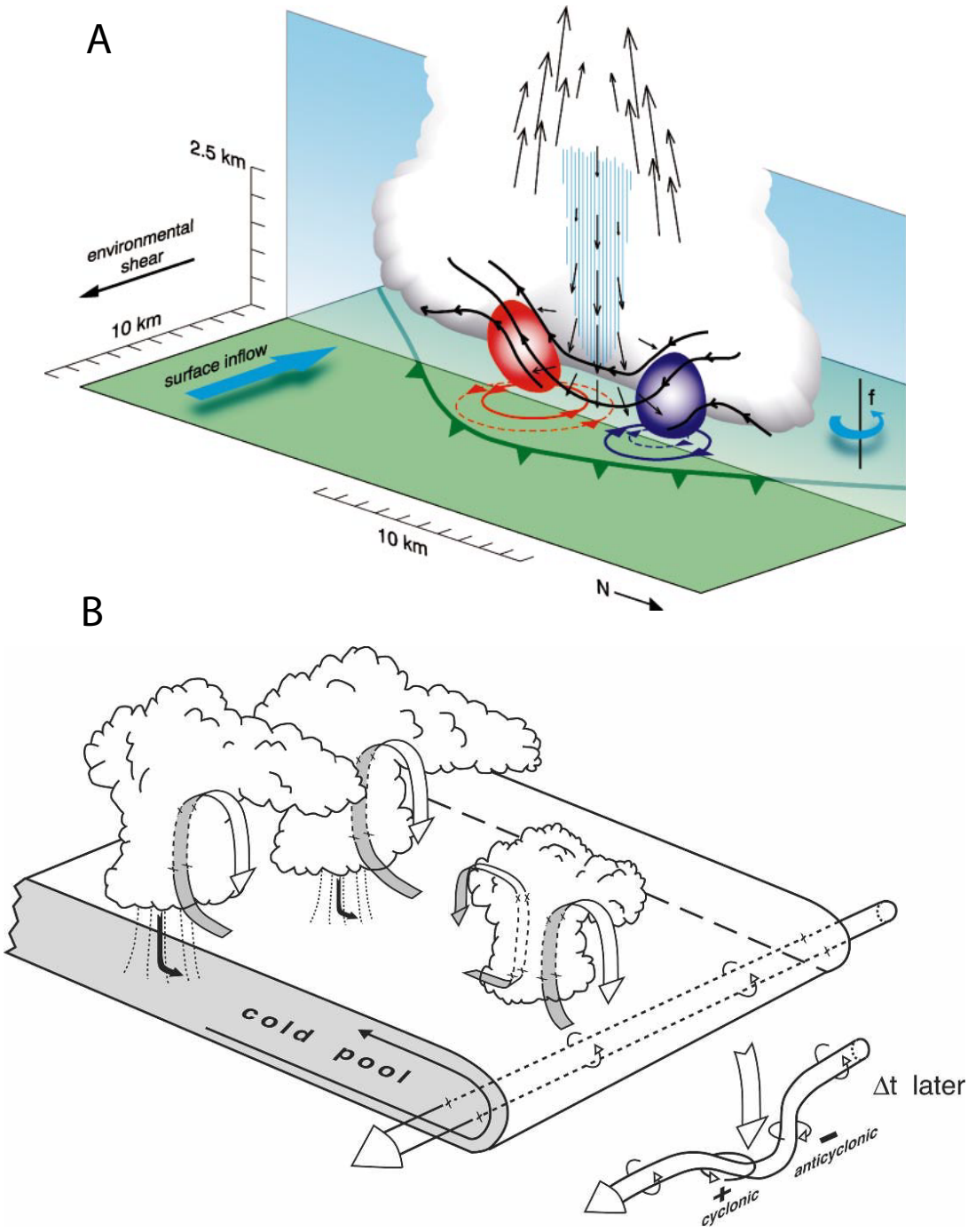

Fig. 8. Two conceptual models of the development of vorticity couplets via downward tilting of vortex lines. (a) Early stage conceptual model from Trapp and Weisman (2003), a rainy downdraft tilts baroclinically-generated vortex lines (black lines) downward to create cyclonic (red shading and lines) and anti-cyclonic (blue shading and lines) vertical vorticity. The green boundary represents the system gust front. (b) From Wakimoto et al. (2006b), downward tilting of vortex lines (tube at the edge of the cold pool) by mechanically forced downdrafts (downward pointing white arrows). This mechanical tilting of vortex lines results in a vortex couplet with the same orientation as that of (a).

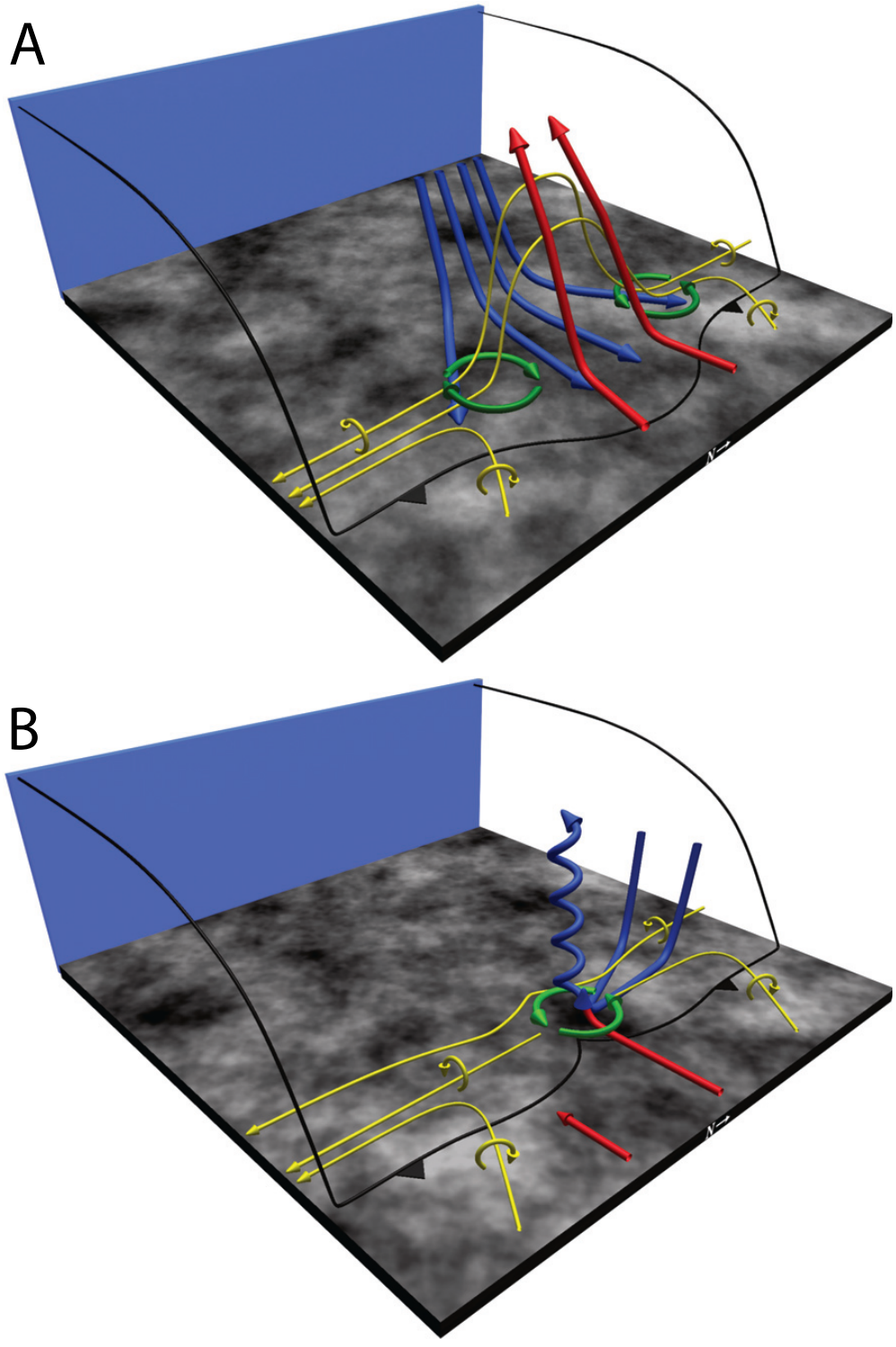

Fig. 9. Two Schematic for mesovortexgenesis from Atkins and St. Laurent (2009b). In (A), system-generated baroclinic vorticity (gold) is tilted upward by an updraft (red) at the leading edge of the cold pool (black). A vortex couplet (green) straddles the downdraft (blue) and updraft. In (B), a cyclonic-only mesovortex is generated by vorticity tilting in a downdraft along the gust front and subsequent rising motion.

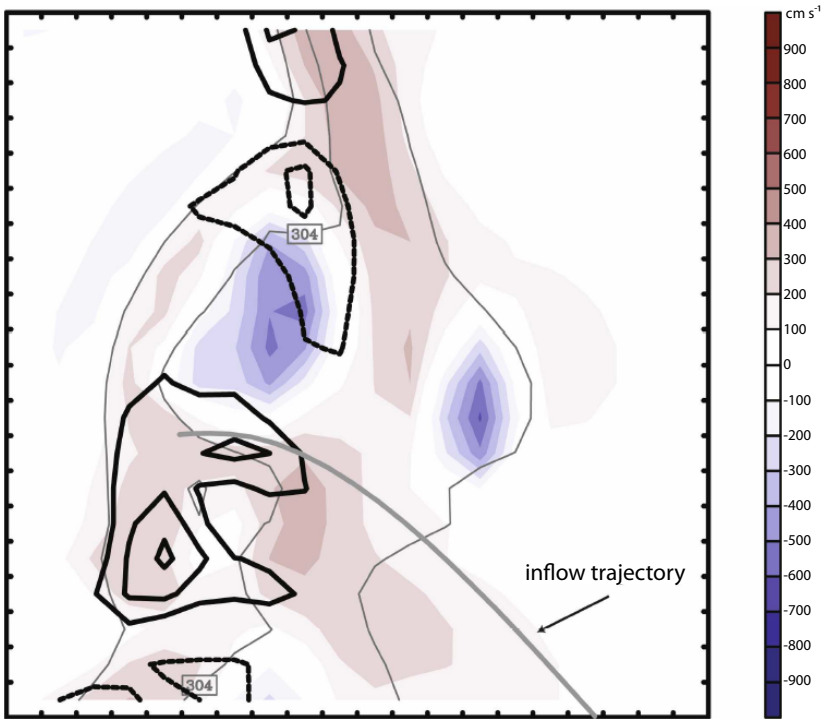

Fig. 10. Simulated vorticity couplet straddling a low-level downdraft at 400 m AGL. Cyclonic vorticity (solid black lines) is south of anti-cyclonic vorticity (dash black lines). Vertical velocity is shaded (cm s^{-1}). Light gray lines are potential temperature isotherms. [From Wheatley and Trapp (2008)].

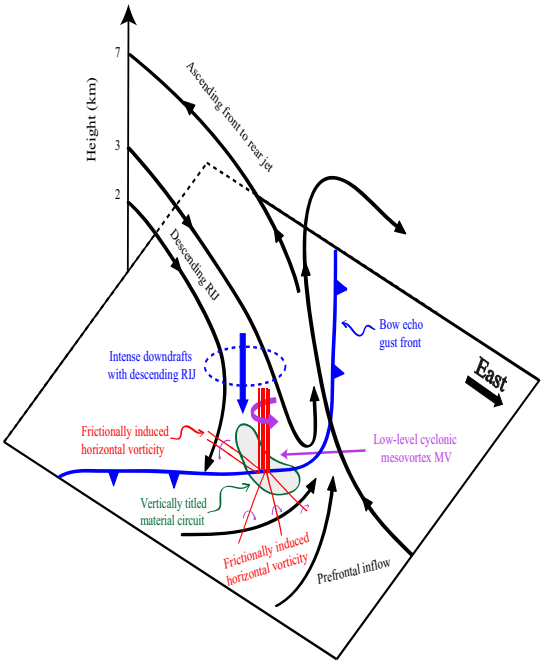

Fig. 11. Schematic from Xu et al. (2015a) showing mesovortexgenesis near the apex of a large bow echo. Red lines denote vortex lines. The mesovortex location is marked by the curved purple arrow. A material circuit enclosing the mesovortex is marked in green and shaded in grey.

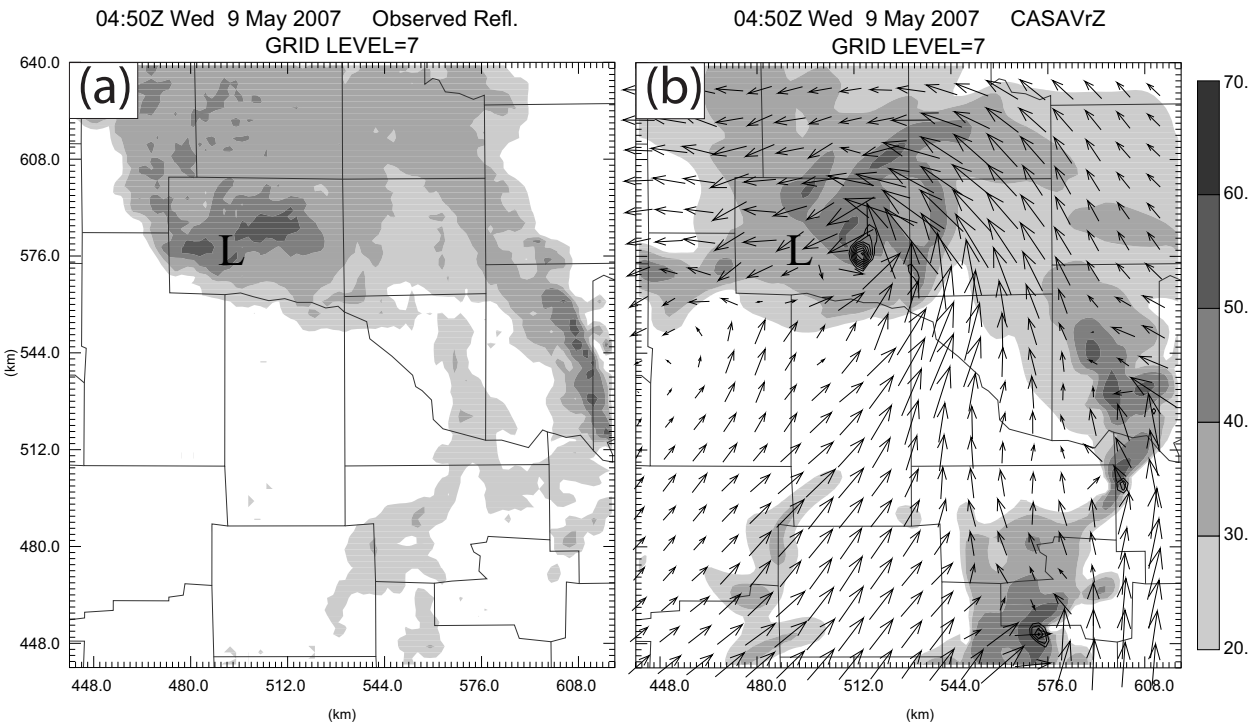

Fig. 12. Reflectivity at grid level 7 (~1 km AGL) at 0450 UTC 9 May 2007 (a) observed radar mosaic and (b) 2 hr 50 min simulation that assimilated data from the WSR-88D and CASA radars. 'L' marks the approximate location of the observed line-end vortex. The vectors and contours in (b) are the horizontal wind and vertical vorticity, respectively. [Adapted from Schenkman et al. (2011a)].

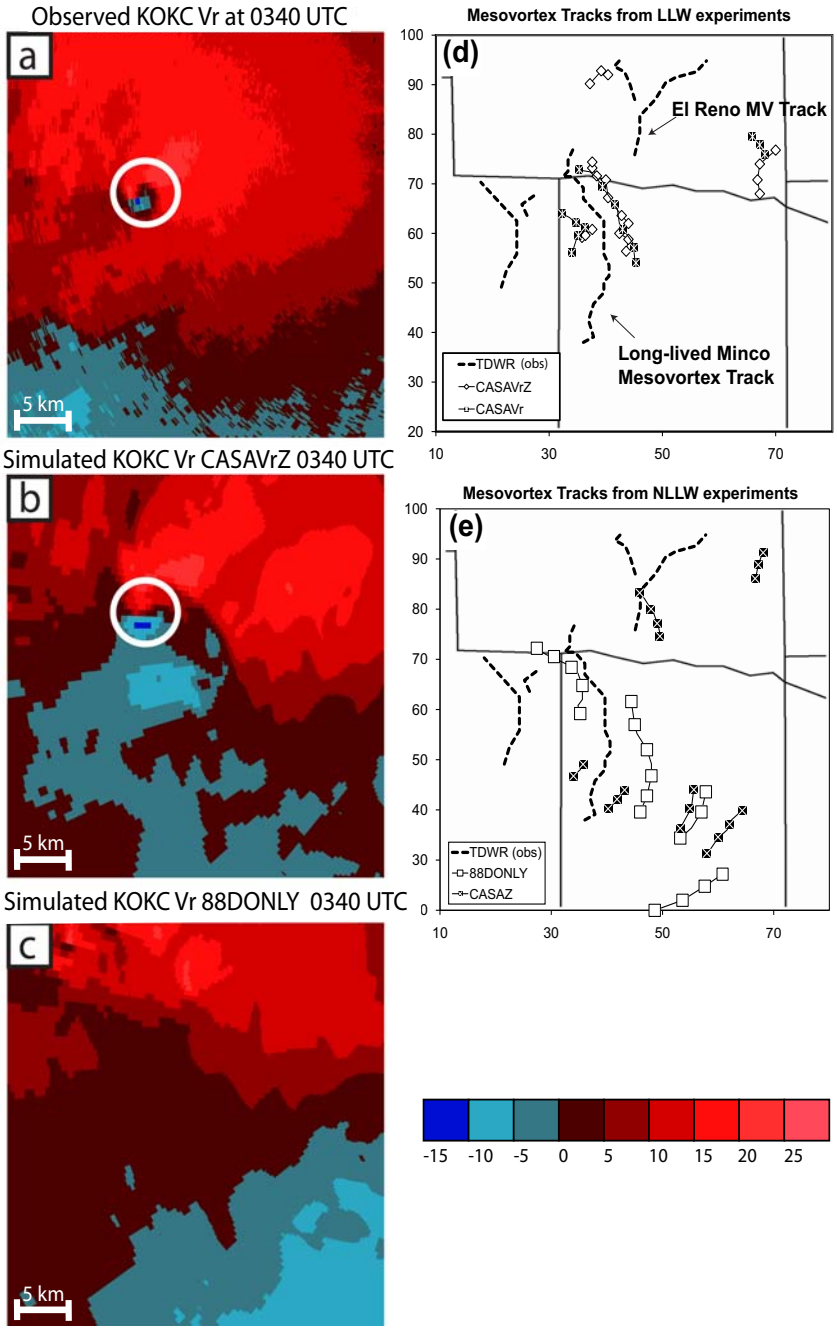

Fig. 13. (a) Observed radar radial velocity observed by the KOKC TDWR at 0340 UTC 9 May 2007. Simulated radar radial velocity from the KOKC TDWR at 340 UTC 9 May 2007 from (b) experiments that assimilated radial velocity from CASA and (c) experiments that only assimilated WSR-88D data. The panels on the right plot observed mesovortex tracks (dashed line) and simulated mesovortex tracks from (d) experiments that assimilated CASA radial velocity data and (e) those that assimilated WSR-88D data only. [Adapated from Schenkman et al. (2011b)].

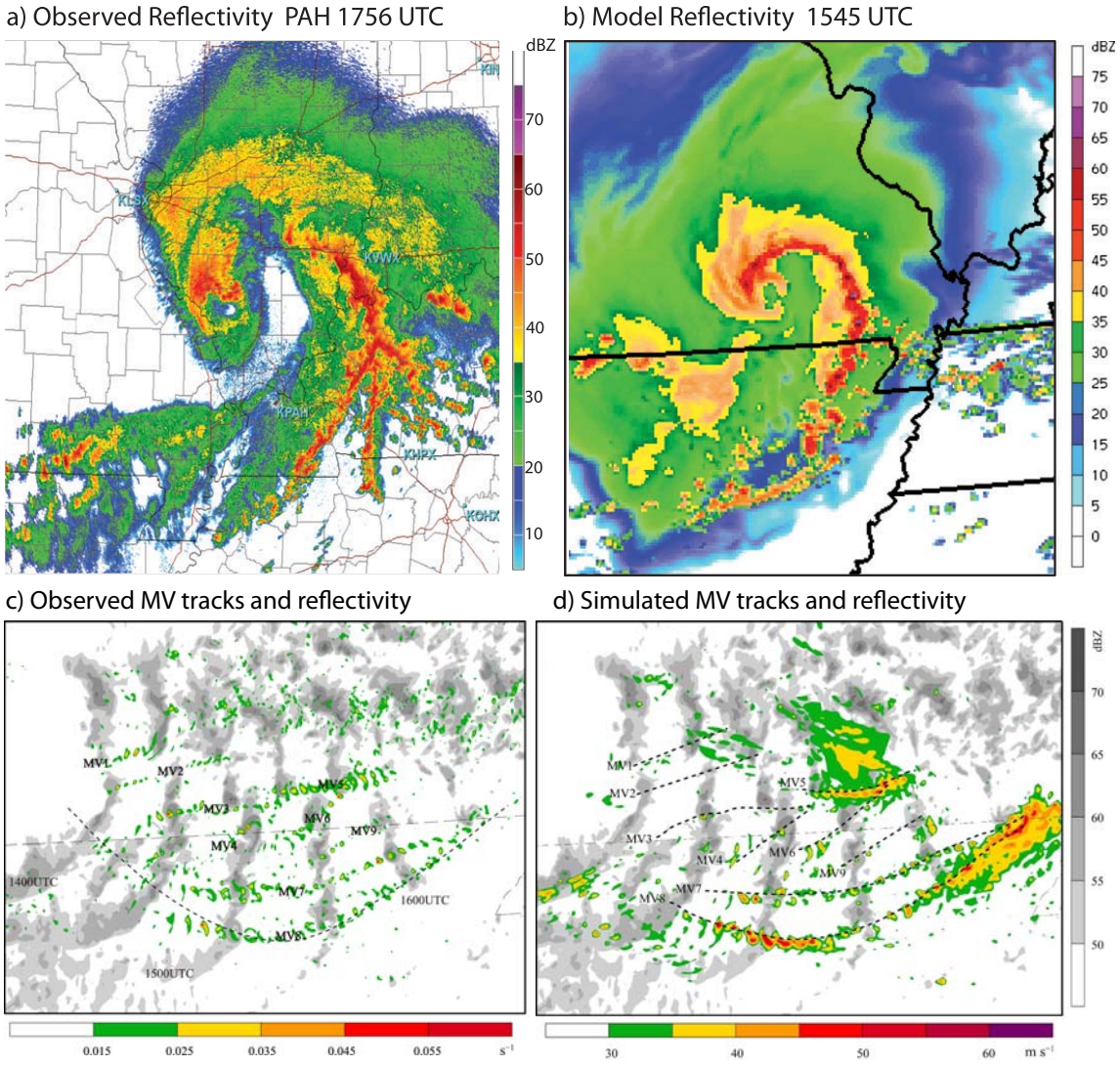

Fig. 14. (a) Observed reflectivity from KPAH at 1756 UTC 8 May 2009. (b) Simulated reflectivity at 1545 UTC 8 May 009. [From Weisman et al. (2013)]. Reflectivity (grayscale shading) and (c) Observed mesovortex tracks and (d) simulated mesovortex tracks [Adapted from Xu et al. (2015b)]. The color shading represents absolute vertical vorticity in (c) and wind speed in (d).